International Journal of Thermal Sciences 48 (2009) 1068–1080

Contents lists available at ScienceDirect

International Journal of Thermal Sciences

www.elsevier.com/locate/ijts

Steady finite Rayleigh number convective flows in a porous medium with internal heat generation

L.R. Mealey, J.H. Merkin *

Department of Applied Mathematics, University of Leeds, Leeds, LS2 9JT, UK

ARTICLE INFO

Article history:
Received 31 July 2008
Received in revised form 20 October 2008
Accepted 21 October 2008
Available online 8 November 2008

Keywords:
Natural convection
Porous media
Darcy's law
Local heat generation
Finite Rayleigh number

ABSTRACT

The steady convective flow within a square region filled with a fluid-saturated porous medium having internal heat generation at a rate proportional to a power of the temperature difference is considered. Three dimensionless parameters are identified, a Rayleigh number Ra, a heating rate parameter γ and the exponent p in the local heating term. The case $Ra = 0$ is considered first, where a critical value γ_c is found, such that there are solutions possible only for $\gamma \leqslant \gamma_c$. This case also identifies a value γ_0, where there is a change in the maximum temperatures $T_{\max}$ achieved. For $\gamma > \gamma_0$, $T_{\max} > 1$ and temperatures above the heated wall value can be generated. Numerical results for $Ra > 0$ are obtained, also showing the existence of a critical value γ_c and a value γ_0. These results show that, for larger values of Ra, boundary layers develop on the vertical walls with a weak eddy flow in the central region. They also show that significantly higher temperatures than the heated wall can be generated by the internal heating, particularly for the larger values of γ.

1. Introduction

There are many practical applications which involve the transport and storage of materials that have a porous nature. Convective flows can develop within these materials if they are subject to some form of external heating. These flows can arise naturally within the porous environment (free convection) or be part of some more extensive heat and mass transfer process (forced or mixed convection), for example, if the porous material is exposed to an external cooling mechanism. Many of these applications are fully discussed and reviewed in the recent books by Nield and Bejan [1], Ingham and Pop [2,3], Vafai [4], Pop and Ingham [5] and Ingham et al. [6]. There are also situations of considerable practical importance where the porous material provides its own source of heat. This gives an alternative way in which a convective flow can be set up through the local heat generation within the porous material. Such a situation can arise through radioactive decay or through, in the present context, a relatively weak exothermic reaction taking place within the porous material. This can happen in the self-induced combustion of coal stockpiles [7,8] and in the storage or transport of organic materials. Bagasse (cellulose waste left after the extraction of juices from sugar cane) has documented cases of self-combustion, as studied by [9–11]. There are also restrictions on the storage of organic materials on ships, for example, pistachio nuts [12].

We model this situation by assuming that the rate of local heat generation within the porous material is proportional to $(T - T_c)^p$, where T is the local temperature and T_c is some constant reference temperature. We further restrict attention to the case $p \geqslant 1$. We consider a two-dimensional, square region with one vertical wall heated to a temperature T_h above that of the reference temperature T_c, the temperature of the other vertical wall. The top and bottom walls are assumed to be thermally insulated. We find that the flow and heat transfer depend on the Rayleigh number Ra and a heat generation parameter γ, as well as the local-heating exponent p. A consideration of the case when $Ra = 0$ reveals that there is a critical value γ_c of γ, dependent on p, such that (steady) solutions exist only for $\gamma < \gamma_c$. This situation also applies when $Ra > 0$, our numerical integrations of the governing equations show that, for a given exponent p, (steady) solutions can exist only for a finite range of Ra and γ.

Previous studies of convective flows in porous media within rectangular enclosures, without the local heat generation effects, are reviewed in [1–4]. Other geometries have also been treated, for example Mahmud and Fraser [13] have looked at flows in a circular enclosure with a temperature differential between the left and right walls. Marcoux et al. [14] have considered flows in annular enclosures, and Rathish Kumar and Shalini [15] have modelled an enclosure with a wavy wall. Singh et al. [16] considered a more generalised form of enclosure with arbitrary geometry.

There have been relatively few previous treatments of convective flows in finite enclosures which also include internal heat generation effects and these have assumed a uniform heating rate within the porous material. Rao and Wang [17] and Haajizadeh

* Corresponding author. Tel.: +113 343 5108; fax: +113 343 5090.
E-mail address: amtjhm@maths.leeds.ac.uk (J.H. Merkin).

1290-0729/$ – see front matter
doi:10.1016/j.ijthermalsci.2008.10.008

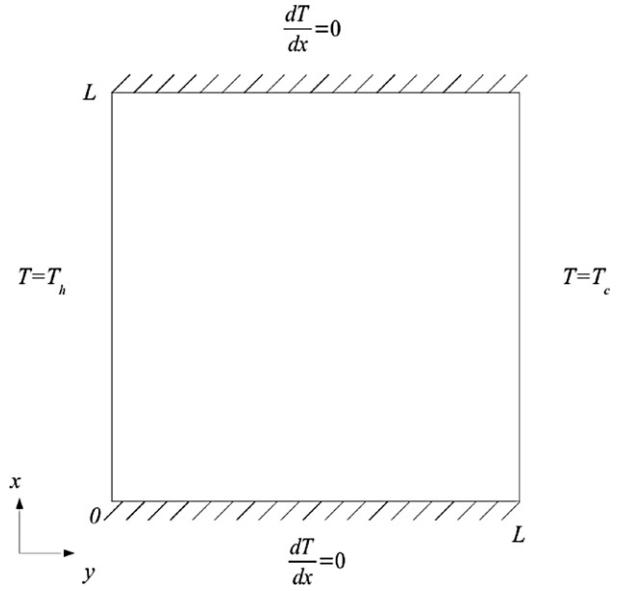

Fig. 1. Schematic representation of the model.

et al. [18] considered a uniform heat generation term across an enclosure with isothermal vertical walls and adiabatic horizontal walls. Stewart et al. [19] modelled the case where the lower half of a rectangular container was adiabatic and the upper half was isothermal. Joshi et al. [20] have given an analytic solution for small Rayleigh number for a finite container with isothermal walls, again for uniform heat generation within the porous medium. Boundary-layer (large Rayleigh) flows in porous media where there is also internal heat generation have been treated by Magyari et al. [21,22]. Here we consider the effects of having a non-uniform heat generation, with the rate of production of heat related to the local temperature difference.

2. Equations

We consider the steady, two-dimensional natural convection flow in a square region filled with a fluid-saturated porous medium, see Fig. 1. The co-ordinate system employed is also depicted in this figure. The top and bottom surfaces of the convective region are assumed to be thermally insulated, the face $\bar{y} = \ell$ is held at the constant reference temperature T_c and the face $\bar{y} = 0$ has a constant prescribed temperature T_h above T_c. Heat is also generated internally within the porous medium at a rate proportional to $(T - T_c)^p$ $(p \geqslant 1)$, where T is the local temperature. The fluid and porous medium properties are assumed to be constant except for the variation of density in the buoyancy term in Darcy's equation for the fluid flow (Boussinesq approximation). The porous medium is taken to be homogeneous and isotropic. Under these assumptions, the equations governing our model are, see for example [1,2,4],

$$\frac{\partial^2 \overline{\psi}}{\partial \bar{x}^2} + \frac{\partial^2 \overline{\psi}}{\partial \bar{y}^2} = \frac{gK\beta}{\nu}\frac{\partial T}{\partial \bar{y}} \tag{1}$$

$$\frac{\partial \overline{\psi}}{\partial \bar{y}}\frac{\partial T}{\partial \bar{x}} - \frac{\partial \overline{\psi}}{\partial \bar{x}}\frac{\partial T}{\partial \bar{y}} = \alpha_m\left(\frac{\partial^2 T}{\partial \bar{x}^2} + \frac{\partial^2 T}{\partial \bar{y}^2}\right) + G(T - T_c)^p \tag{2}$$

where K is the permeability of the porous media, ν the kinematic viscosity, β the coefficient of thermal expansion, g the acceleration due to gravity, α_m the effective thermal diffusivity and G is a measure of the local heat generation. The streamfunction ψ, introduced to satisfy the continuity equation, gives the velocity components as $u = \partial\overline{\psi}/\partial\bar{y}$, $v = -\partial\overline{\psi}/\partial\bar{x}$. Eqs. (1), (2) are to be solved subject to the boundary conditions that

$$\begin{aligned}
&\text{on } \bar{x} = 0,\ \bar{x} = \ell, && \overline{\psi} = 0, && \frac{\partial T}{\partial \bar{x}} = 0 \quad (0 < \bar{y} < \ell)\\
&\text{on } \bar{y} = \ell, && \overline{\psi} = 0, && T = T_c \quad (0 < \bar{x} < \ell)\\
&\text{on } \bar{y} = 0, && \overline{\psi} = 0, && T = T_h \quad (0 < \bar{x} < \ell)
\end{aligned} \tag{3}$$

We make Eqs. (1)–(3) dimensionless by writing

$$\overline{\psi} = \frac{g\beta K\ell\Delta T}{\nu}\psi, \qquad \theta = \frac{T - T_c}{\Delta T}$$

$$x = \frac{\bar{x}}{\ell}, \qquad y = \frac{\bar{y}}{\ell} \quad (\text{where } \Delta T = T_h - T_c > 0) \tag{4}$$

This results in the non-dimensional equations for our model as

$$\frac{\partial^2 \psi}{\partial x^2} + \frac{\partial^2 \psi}{\partial y^2} = \frac{\partial \theta}{\partial y} \tag{5}$$

$$Ra\left[\frac{\partial \psi}{\partial y}\frac{\partial \theta}{\partial x} - \frac{\partial \psi}{\partial x}\frac{\partial \theta}{\partial y}\right] = \frac{\partial^2 \theta}{\partial x^2} + \frac{\partial^2 \theta}{\partial y^2} + \gamma\theta^p \tag{6}$$

subject to the boundary conditions that

$$\begin{aligned}
&x = 0,\ x = 1, && \psi = 0, && \frac{\partial \theta}{\partial x} = 0 \quad (0 < y < 1)\\
&y = 1, && \psi = 0, && \theta = 0 \quad (0 < x < 1)\\
&y = 0, && \psi = 0, && \theta = 1 \quad (0 < x < 1)
\end{aligned} \tag{7}$$

In the above

$$Ra = \frac{g\beta K\ell\Delta T}{\alpha_m \nu} \quad (\text{Rayleigh number})$$

$$\gamma = \frac{G\ell^2(\Delta T)^{p-1}}{\alpha_m} \quad (\text{heating parameter})$$

Our formulation (4) gives, from (5), a convective flow even at $Ra = 0$. An alternative formulation could be to write $\psi = Ra^{-1}\tilde{\psi}$ (or $\overline{\psi} = \alpha_m\tilde{\psi}$). In the $(\theta, \tilde{\psi})$ variables there is then no convective flow at $Ra = 0$, with a flow arising at $O(Ra)$ for Ra small, consistent with the scaling (4). As a measure of our solution we use the total (dimensionless) heat Q generated within the convective region given by

$$Q = \int_0^1\int_0^1 \theta(x, y)\,dx\,dy \tag{8}$$

For general values of the parameters Ra, γ and p, Eqs. (5)–(7) have to be solved numerically, and we describe our numerical results in detail below. However, we can gain some insight into the nature of the problem by considering the case when $Ra = 0$ and this what we discuss next.

3. Case $Ra = 0$

When $Ra = 0$, Eq. (6) for the temperature θ becomes independent of that for the flow (5). In this case $\theta = \theta(y)$ and (6), (7) reduce to the boundary-value problem

$$\theta'' + \gamma\theta^p = 0, \quad \theta(0) = 1, \quad \theta(1) = 0 \tag{9}$$

where primes denote differentiation with respect to y.

When $p = 1$, Eq. (9) can be solved as

$$\theta(y) = \frac{\sin\sqrt{\gamma}(1 - y)}{\sin\sqrt{\gamma}} \quad (\gamma > 0)$$

$$\theta(y) = 1 - y \quad (\gamma = 0) \tag{10}$$

with (8) then giving for this case

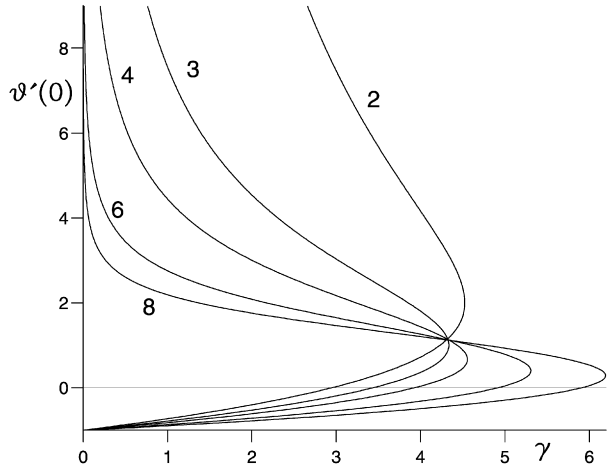

Fig. 2. Values of $\theta'(0)$ for $Ra = 0$ plotted against γ obtained from the numerical solution of (9) for the values of p labelled on the figure.

$$Q = \frac{1-\cos\sqrt{\gamma}}{\sqrt{\gamma}\sin\sqrt{\gamma}} \quad (\gamma > 0)$$

$$Q = \frac{1}{2} \quad (\gamma = 0) \tag{11}$$

From (10) or (11) we see that the solution becomes singular as $\gamma \to \gamma_c = \pi^2$ and this puts an upper bound on the value of γ for which we can obtain solutions for this case.

For other values of p Eq. (9) has an implicit solution in terms of hypergeometric functions, however, we find it more straightforward to solve (9) numerically. We started our numerical solutions with the solution for $\gamma = 0$ (the solution given in (10) for $\gamma = 0$ holds for all p). To determine any possible turning points (saddle-node bifurcations) in the solution, we gave $\theta'(0)$ a prescribed value, starting with the value $\theta'(0) = -1$ for $\gamma = 0$, and incremented this value in small steps. We used a standard boundary-value problem solver (D02AGF in the NAG library [23]) to calculate the corresponding value of γ. The results for several values of p are shown in Fig. 2 as plots of $\theta'(0)$ against γ. The main features to note about the curves shown in Fig. 2 are that there is an upper bound γ_c on γ for the existence of a solution, with the value of γ_c being dependent on p. For $\gamma < \gamma_c$ there are two solution branches with a saddle-node bifurcation at γ_c. The value of γ_c initially decreases as p is increased from $p = 1$ before increasing again for the larger values of p. The lower branch solutions are the ones found in our numerical simulations, suggesting that this is the stable solution branch, the saddle-node bifurcation at γ_c giving an unstable upper branch. Fig. 2 also indicates that there is a value γ_0 of γ (dependent on p) at which $\theta'(0) = 0$ on the lower solution branch. For larger values of γ on this branch, $\theta'(0) > 0$ and $\theta(y)$ achieves a maximum value above the heated wall value of $\theta(0) = 1$ within the solution domain.

The value of γ_c can be determined by solving (9) for $\theta_c(y)$ at γ_c together with the homogeneous problem

$$\theta_1'' + p\gamma_c\theta_c^{p-1}\theta_1 = 0$$

$$\theta_1(0) = \theta_1(1) = 0, \qquad \theta_1'(0) = 1 \tag{12}$$

the final boundary condition on θ_1 being applied to force a non-trivial, solution. Eq. (12) can be derived by assuming that $\gamma = \gamma_c + O(|\gamma - \gamma_c|^2)$ near γ_c, with (12) then being the term of $O(|\gamma - \gamma_c|)$ in an expansion for $\theta(y;\gamma)$ in powers of $|\gamma - \gamma_c|$. Now, from (9),

$$\theta_c'(y)^2 = \theta_c'(1)^2 - \frac{2\gamma_c}{p+1}\theta_c(y)^{p+1} \tag{13}$$

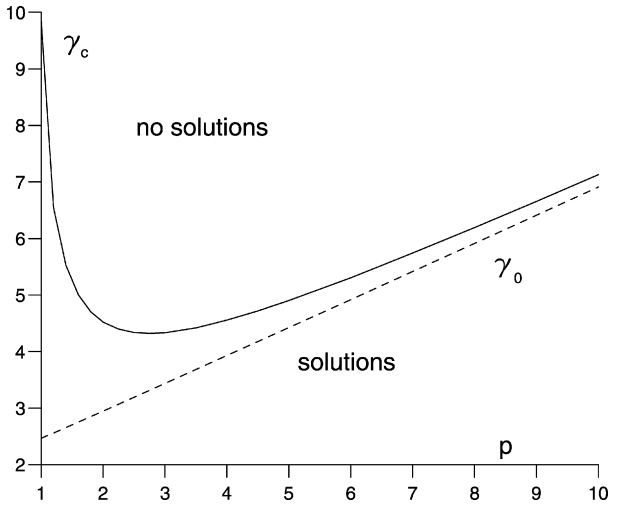

Fig. 3. Values of γ_c (full line) for $Ra = 0$ plotted against p, obtained from solving (9) subject to conditions (17). The region of the γ–p parameter plane where there are solutions to (9) is labelled on the figure. The values of γ_0, where $\theta'(0) = 0$ on the lower solution branch are shown by the broken line.

from which it follows that

$$\theta_c'(0)^2 = \theta_c'(1)^2 - \frac{2\gamma_c}{p+1} \tag{14}$$

In fact, expressions (13), (14) hold for all solutions to (9).

The general solution to Eq. (12) is seen to be

$$\theta_1(y) = A_1\theta_c'(y) + B_1\left(y\theta_c'(y) + \frac{2}{p-1}\theta_c(y)\right) \quad (p > 1) \tag{15}$$

for constants A_1, B_1. Applying the boundary conditions given in (12) then gives

$$A_1\theta_c'(0) + \frac{2}{p-1}B_1 = 0$$

$$(A_1 + B_1)\theta_c'(1) = 0 \tag{16}$$

from which it follows that

$$\theta_c'(0) = \frac{2}{p-1} \quad (p > 1)$$

$$\theta_c'(1)^2 = \frac{4}{(p-1)^2} + \frac{2\gamma_c}{p+1} \tag{17}$$

Applying these conditions in (9) enables γ_c to be determined and a graph of γ_c against p is shown in Fig. 3 (by the full line). This figure shows that γ_c has a minimum value of $\gamma_c \simeq 4.2$ at $p \simeq 2.8$, consistent with the results shown in Fig. 2, and that γ_c increases linearly for the larger values of p. There is a difference between the cases $p = 1$ and $p > 1$ in that, for $p = 1$, the solution to (9) breaks down with $Q \to \infty$ and $\theta'(0) \to \infty$ as $\gamma \to \gamma_c$, from (10), (11), whereas for $p > 1$, these quantities remain finite at the saddle-node bifurcation at γ_c.

To see how the behaviour for the larger values of p arises we can obtain a solution of (9) valid for p large. In this case there is an outer region where y is of $O(1)$ and $\theta(y) < 1$ so that the reaction term θ^p is negligible for p large. The solution in this outer region is, to leading order, $\theta(y) = 1 - y$, chosen to satisfy the boundary condition at $y = 1$ and to match at leading order with the inner region. For this inner region we scale γ by $\gamma = p\overline{\gamma}$, where $\overline{\gamma}$ is of $O(1)$ for p large and then put $Y = yp, \theta = 1 + Up^{-1}$. This gives, again at leading order,

$$U'' + \overline{\gamma}e^U = 0, \qquad U(0) = 0$$

$$U \sim -Y \quad \text{as } Y \to \infty \tag{18}$$

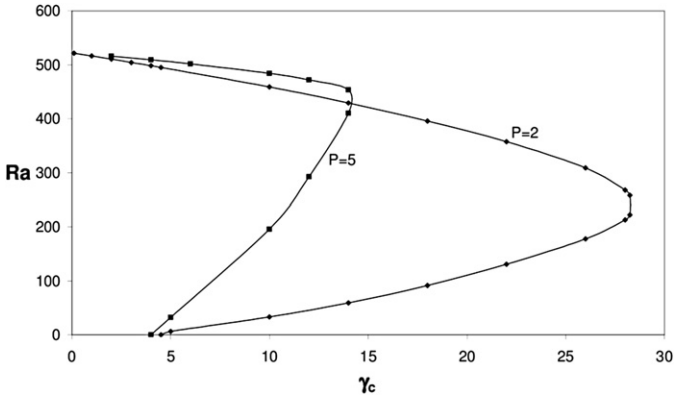

Fig. 4. The effect of Ra on γ_c, showing γ_c plotted against Ra for $p = 2, 5$. ■ denotes the values at which numerical integrations were performed.

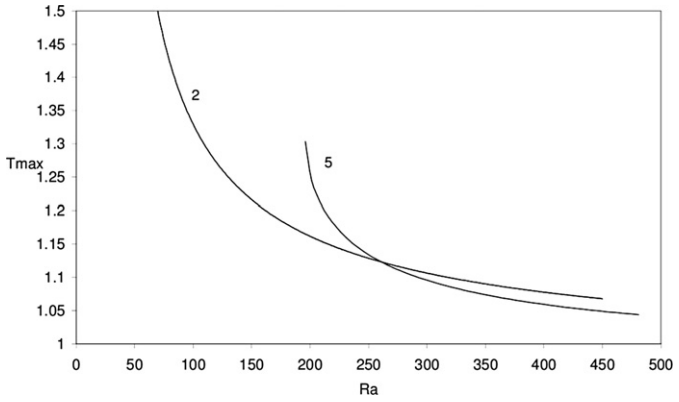

Fig. 5. The maximum temperature $T_{\max}$ plotted against Ra for $\gamma = 10.0$ with $p = 2, 5$.

on matching with the outer region. Eq. (18) can be expressed as, on satisfying the matching condition in (18),

$$U'(Y)^2 = 1 - 2\overline{\gamma}e^U \tag{19}$$

The boundary condition on $Y = 0$ then gives

$$U'(0)^2 = 1 - 2\overline{\gamma} \quad \left(\text{for } \overline{\gamma} \leqslant \frac{1}{2}\right) \tag{20}$$

This is in line with expression (14) and gives

$$\overline{\gamma}_c = \frac{1}{2} \quad \text{or} \quad \gamma_c \sim \frac{p}{2} + \cdots \quad \text{as } p \to \infty \tag{21}$$

This result is consistent with the slope of the curve for γ_c plotted in Fig. 3 for the larger values of p. Our solution for p large gives $\theta'(0) \sim -1 + \frac{\gamma}{p} + \cdots$, showing that the effect of the heat generation becomes less significant as the power p increases. For $\overline{\gamma} < \overline{\gamma_c}$ only small maximum temperatures, of $O(p^{-1})$, above the heated wall temperature are achieved with these maximum temperatures arising close to the heated wall.

For $Ra = 0$ and $p = 1$, the maximum temperature $T_{\max}$ is given by

$$\begin{aligned} &T_{\max} = 1 \quad \text{at } y = 0 \\ &\quad \text{if } \gamma \leqslant \frac{\pi^2}{4} \\ &T_{\max} = \frac{1}{\sin\sqrt{\gamma}} \quad \text{at } y = 1 - \frac{\pi}{2\sqrt{\gamma}} \\ &\quad \text{if } \frac{\pi^2}{4} < \gamma < \pi^2 = \gamma_c \end{aligned} \tag{22}$$

from (10). This gives a value $\gamma_0 = \frac{\pi^2}{4}$ at which the maximum temperature $T_{\max}$ changes from being $T_{\max} = 1$ ($\gamma < \gamma_0$) and located

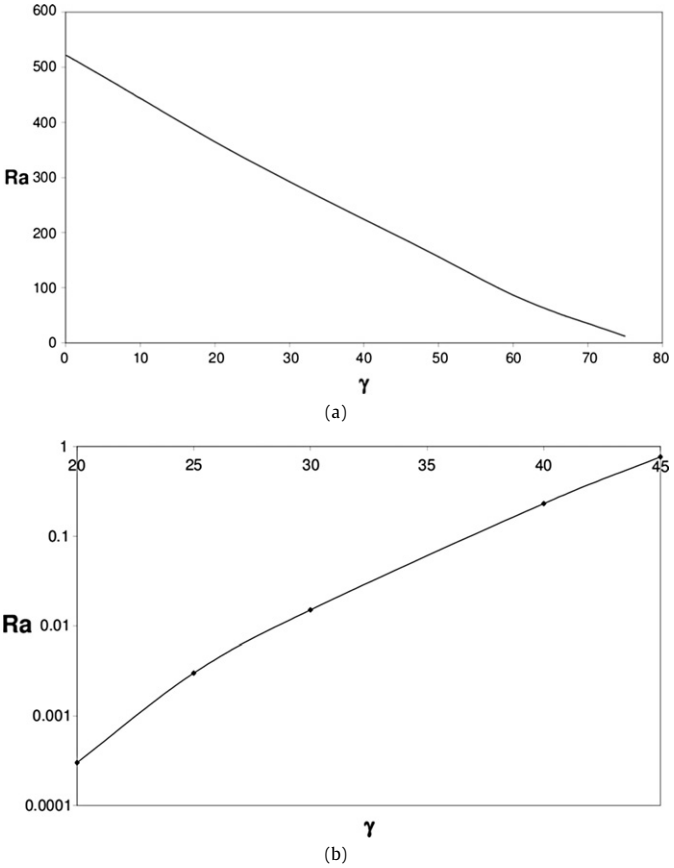

Fig. 6. The values of γ_c plotted against Ra for (a) $p = 1$, (b) $p = 1.1$. ■ denotes the values at which numerical integrations were performed.

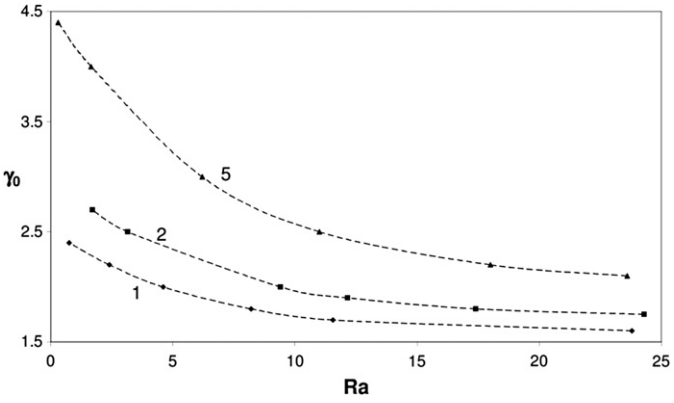

Fig. 7. The values of γ_0, where there is a change from having $T_{\max} = 1$ to having $T_{\max} > 1$ and fluid temperatures above the heated wall value, plotted against Ra for $p = 1.0, 2.0, 5.0$. ■ denotes the values at which numerical integrations were performed.

on the heated wall, $y = 0$, to having $T_{\max} > 1$ ($\gamma > \gamma_0$) now being located within the flow domain. To find γ_0 for other values of p we need to solve (9) subject to the extra condition that $\theta'(0) = 0$. This gives

$$\theta'^2 = \frac{2\gamma_0}{p+1}\left(1 - \theta^{p+1}\right) \tag{23}$$

The condition that $\theta(1) = 0$ then gives the relation

$$\sqrt{\frac{2\gamma_0}{p+1}} = \int_0^1 \frac{d\theta}{(1-\theta^{p+1})^{1/2}} = \frac{\sqrt{\pi}(p+3)}{2(p+1)} \frac{\left(\frac{1}{p+1}\right)!}{\left(\frac{p+3}{2(p+1)}\right)!} \tag{24}$$

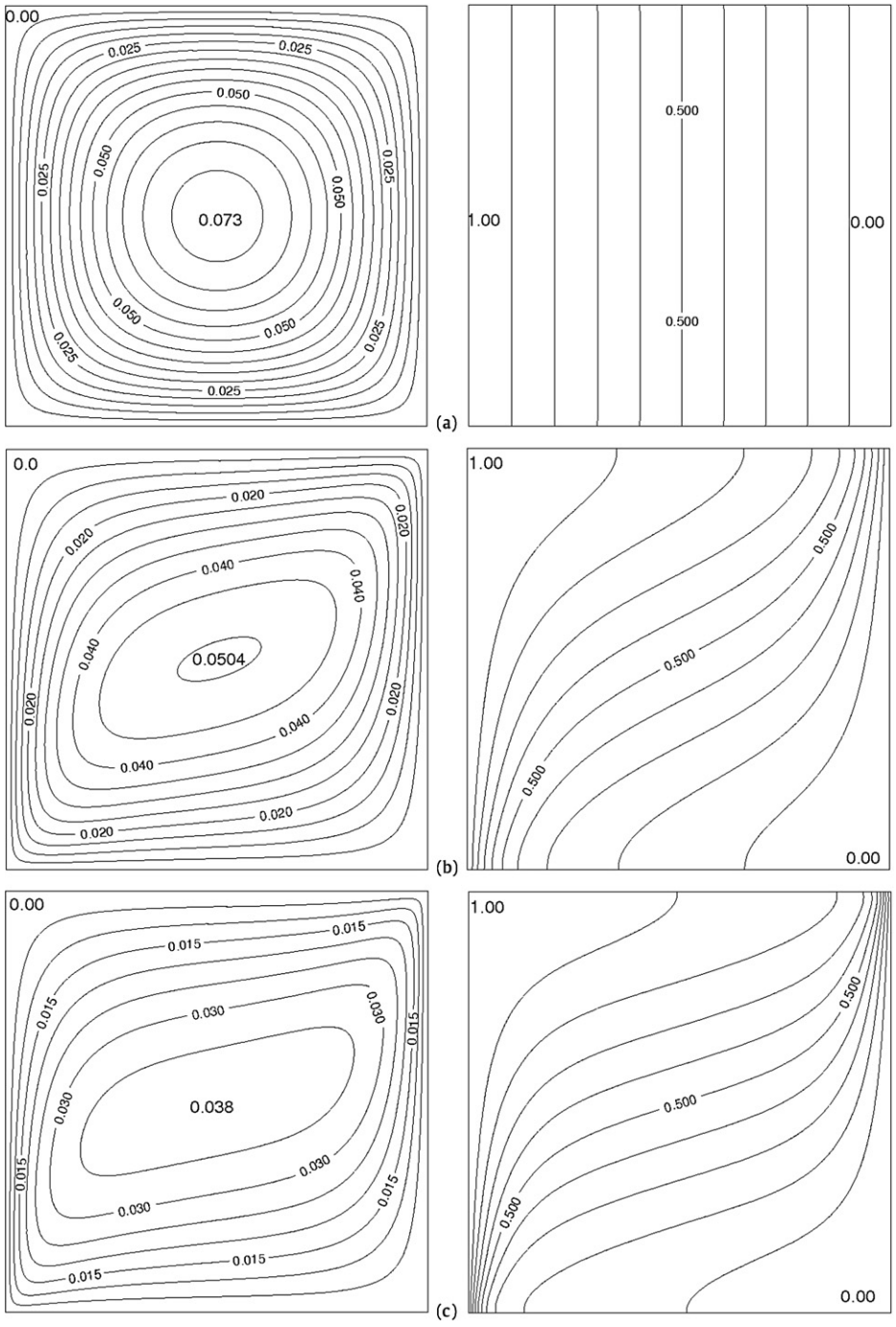

Fig. 8. Contour plots of the stream function and temperature for $\gamma = 0.1$, $p = 1$ and (a) $Ra = 0$, (b) $Ra = 40$, (c) $Ra = 100$, (d) $Ra = 300$, (e) $Ra = 500$.

on expressing the integral in (24) in terms of the Beta Function [24]. We see that $\gamma_0 \sim p/2$ as $p \to \infty$ in line with (19) and (24) gives the value in (22) for γ_0 when $p = 1$. Values of γ_0 are also shown in Fig. 3 (by the broken line), with $\theta'(0)$ being positive above this line in the region where solutions exist. The variation of γ_0 with p is almost linear, with $\gamma_0 \simeq p/2 + 2$ giving a very good approximation.

4. Results for $Ra > 0$

4.1. Numerical method

Eqs. (5)–(7) were solved numerically by first replacing the derivatives by central differences. The resulting sets of finite-difference equations were solved using Gauss–Seidel iteration. For a typical numerical run we used a 100×100 mesh, giving the step sizes $\Delta x = \Delta y = 0.01$. We found that the iterative procedure converged relatively easily with this mesh size. We also performed a few runs with a 200×200 mesh to check accuracy, finding good agreement with runs using a 100×100 mesh for the same parameter values. We also compared our numerical results with those obtained from (9) (and with (10) for $p = 1$) with $Ra = 0$, again finding good agreement. Thus giving confidence in the accuracy of our numerical results.

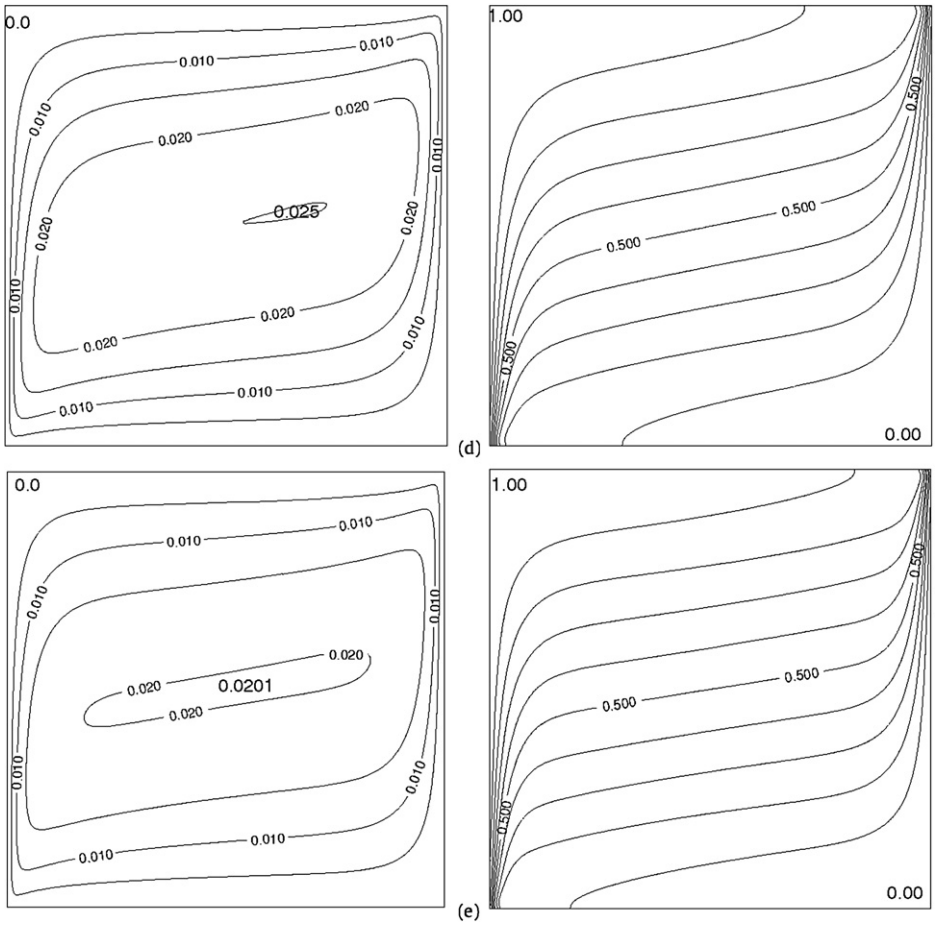

Fig. 8. (*continued*)

4.2. Critical values

For the case with $Ra = 0$ we have identified a critical value γ_c of γ (dependent on p) for the existence of a solution. We started by examining this point for $Ra > 0$ by performing numerical runs, for given values of γ and p, starting at a value of Ra at which we knew there was a solution and increasing Ra in small increments until the numerical procedure failed to converge. As a check on this approach, we used this procedure with $Ra = 0$ to calculate γ_c for several values of p. We found that it gave the same value for γ_c determined previously from solving (12) using a boundary-value problem solver. This gave us confidence that this was a reliable method for finding critical points for $Ra > 0$.

In Fig. 4 we plot γ_c against Ra for $p = 2$ and $p = 5$, with there being a solution for $\gamma \leqslant \gamma_c(Ra)$. In this and similar figures ■ denotes the values at which numerical integrations were performed. The figure shows that γ_c starts at the values shown in Fig. 3 for $Ra = 0$ and then begins by increasing as Ra is increased. For larger values of Ra, γ_c achieves a maximum value, of $\gamma_c \simeq 28.3$ at $Ra \simeq 240$ for $p = 2$ and of $\gamma_c \simeq 14.2$ at $Ra \simeq 450$ for $p = 5$, before decreasing towards zero as Ra is increased still further. Fig. 4 shows that the effect of the flow (having $Ra > 0$ and relatively weak convection) is to increase the range of γ where there is a solution for the smaller values of Ra. However, further increasing the effects of the convective flow (increasing Ra) reduces the range of possible solutions, with there being an upper bound on Ra for the existence of a (steady) solution. The effect of the flow is to reduce the fluid temperatures and, in particular, to reduce the maximum temperature $T_{\max}$ for given values of γ and p. We illustrate this in Fig. 5 with plots of $T_{\max}$ against Ra for $\gamma = 10.0$ and $p = 2, 5$. We note, from Fig. 4, that there is only a limited range of Ra for a solution, that $T_{\max}$ reduces towards the heated wall temperature of $T_{\max} = 1$ as Ra is increased towards its upper bound and that $T_{\max}$ becomes large (though still bounded) at the lower value of Ra for the existence of a solution.

The situation for $p = 1$ is somewhat different to the cases when $p > 1$. We have already seen that there is a difference when $Ra = 0$ in that the temperature remains finite for $p > 1$ but becomes unbounded as $\gamma \to \gamma_c$ when $p = 1$, as can be seen from (10). In Fig. 6a we plot γ_c against Ra for $p = 1$. For the larger values of Ra the behaviour is similar to the previous cases (Fig. 4) with a comparable upper bound on Ra. However, for the smaller values of Ra the situation is markedly different. Now we find that γ_c achieves relatively high values for small, but non-zero, values of Ra, with $\gamma_c \simeq 75$ at $Ra = 0.1$ compared to $\gamma_c = 9.870$ at $Ra = 0$. We considered even smaller values of Ra but were unable to find a 'smooth join' with the result for $Ra = 0$. The temperatures remained finite as γ approached γ_c when $Ra > 0$.

To examine this point a little further, we considered the case with $p = 1.1$. Here we also found an increase in γ_c for small Ra, with for example $\gamma_c = 36.9$ at $Ra = 0.1$, though now we were able to find a smooth join with the value of $\gamma_c = 7.533$ for $Ra = 0$ by taking even smaller values of Ra as can be seen in Fig. 6b where we plot γ_c against Ra for small values of Ra. This figure shows that γ_c decreases rapidly from its value at $Ra = 0.1$ towards the much smaller value for $Ra = 0$.

From the above discussion for $Ra = 0$ we can expect, at least for small values of γ and $Ra > 0$, that the maximum temperature $T_{\max}$ to be at the heated wall ($T_{\max} = 1$) whereas with increased values of γ and Ra we might expect higher temperatures ($T_{\max} > 1$)

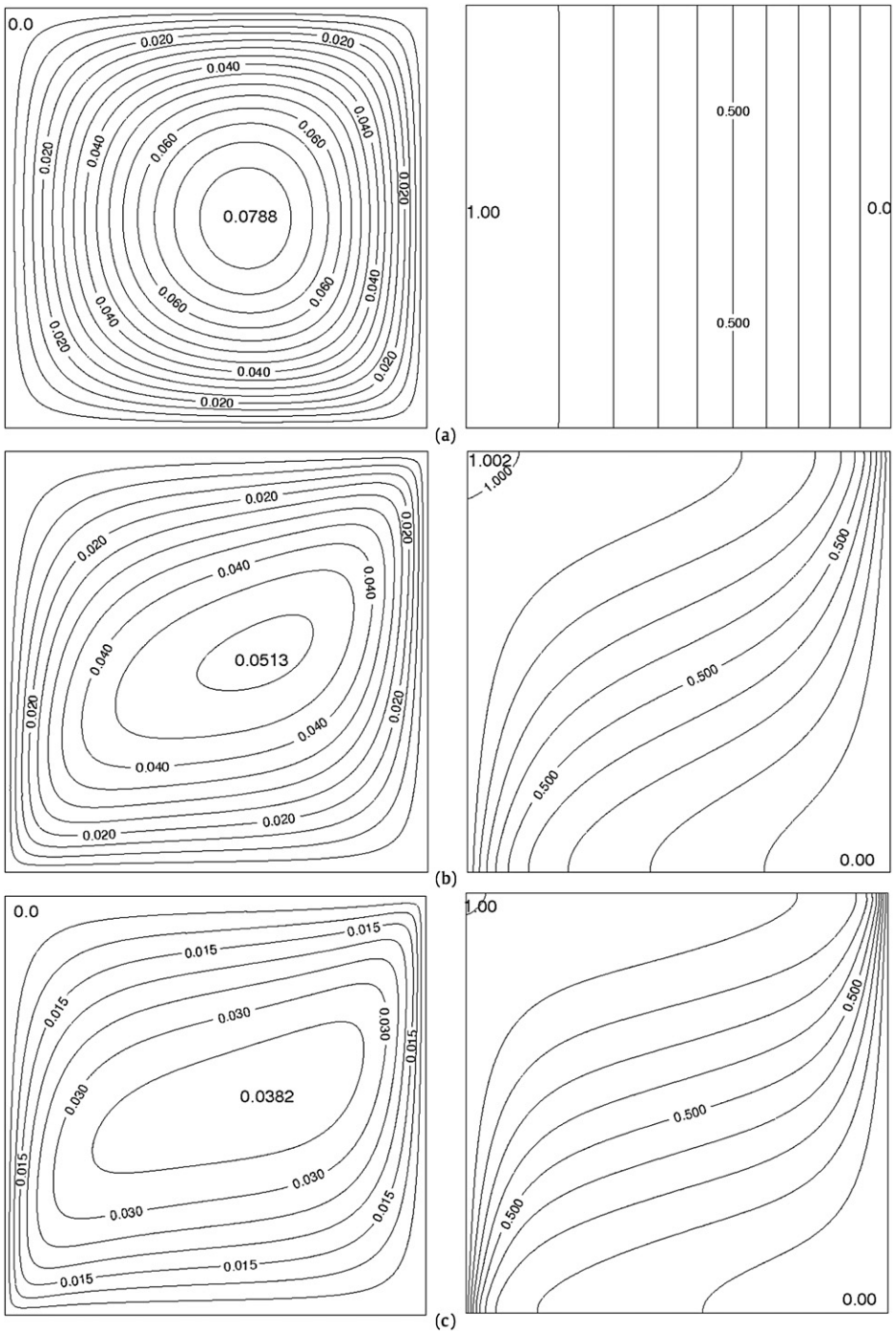

Fig. 9. Contour plots of the stream function and temperature for $\gamma = 2.0$, $p = 1$ and (a) $Ra = 0$, (b) $Ra = 40$, (c) $Ra = 100$, (d) $Ra = 300$, (e) $Ra = 500$.

with these being located within the flow domain. In Fig. 7 we plot γ_0 against Ra for $p = 1, 2, 5$. The values of Ra and γ below these curves are where the maximum temperature $T_{\max} = 1$, located on the heated (vertical) wall with the fluid temperature being everywhere less than this. The values of Ra and γ above these curves are where $T_{\max} > 1$, being located on the upper (insulated) wall with fluid temperatures above the heated wall value now being achieved. This figure shows that increasing the exponent p requires a larger value of γ (increased local heating) before temperatures above $T_{\max} = 1$ are achieved. However, this effect becomes less significant as Ra is increased with, for larger values of Ra, smaller local heating rates being needed to produce temperatures above the heated wall value.

4.3. Numerical results

Here we consider how the convective flow, through varying the Raleigh number Ra, affects the temperature field and the heat transfer. We consider different values for γ representative of the internal heating effect as well as different values for p. We start by considering a case where the effects of the internal heating are relatively weak, namely $\gamma = 0.1$.

4.3.1. Weak heating, $\gamma = 0.1$

In this case we found that $T_{\max} = 1$, located on the heated wall, with the fluid temperatures being less than $T_{\max}$ throughout for all the values of Ra tried up to the critical value of Ra for $p = 1, 2$

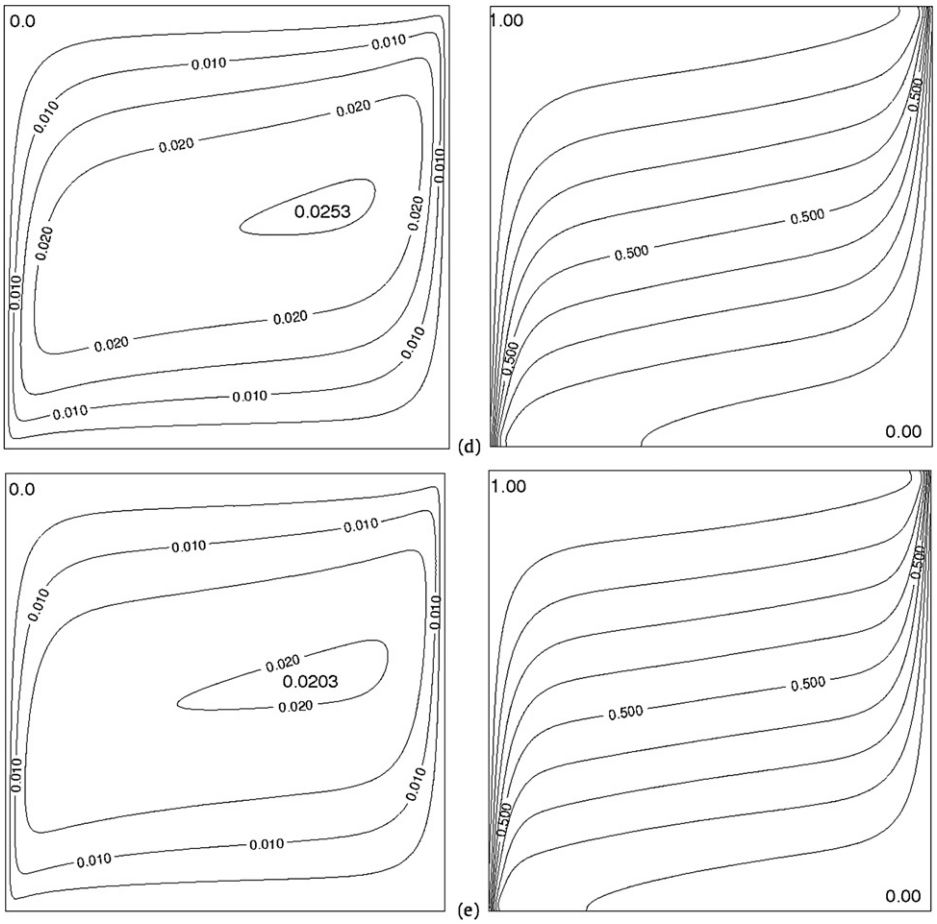

Fig. 9. (*continued*)

and 5. This case is illustrated in Fig. 8 showing temperature and streamline contour plots for a range of values of Ra from $Ra = 0$ to $Ra = 500$ and $p = 1$. Fig. 8 shows how the flow and temperature distribution evolve as Ra is increased. For $Ra = 0$ (Fig. 8a) the temperature is given by (9) (or by (10) for $p = 1$), being dependent only on y with a symmetric eddy flow centred on the mid-point of the domain. As Ra is increased, the isotherms become distorted by the flow, giving higher temperatures in a region towards the top of the heated wall and lower temperatures in the opposite corner. The streamline pattern also becomes distorted with stronger flows developing on the heated ($y = 0$) and cooled ($y = 1$) walls (Figs. 8b and 8c for $Ra = 40$ and $Ra = 100$).

At higher values of Ra (Fig. 8d for $Ra = 300$) the extent of these high, $T \simeq 1$, and low, $T \simeq 0$, temperature regions increase in size. A strong upflow develops on the heated wall and a strong downflow on the cooled wall with only a weak eddy flow in the central region. These convective effects become more pronounced at higher values of Ra (Fig. 8e for $Ra = 500$). Here boundary layers form on both the heated and cooled vertical walls. The temperature distribution in the central region becomes strongly dependent on x and almost independent of y (compare with Fig. 8a) and the flow in this region becomes almost stagnant. We note that very similar behaviour was seen for the other values of p tried for this value of γ.

4.3.2. Moderate heating, $\gamma = 2.0$

Since, from (22) or (24), $\gamma_0 > 2.0$ for all $p \geqslant 1$ with $Ra = 0$, we have $T_{\max} = 1$ for $Ra = 0$ with this maximum temperature being located on the heated wall, $y = 0$. We illustrate this case with contour plots for $p = 1$ for a range of Ra. The situation for $Ra = 0$ (Fig. 9a) is similar to the previous case, though now, as expected from (10), the temperature and streamfunction profiles are more distorted towards the cooled wall. For $Ra = 40, 100$ (Figs. 9b, 9c), the picture is in general similar to the previous case but now having slightly stronger flow rates. There is a difference with the previous case in that there is a small region close to the top of the heated wall where the fluid temperature is slightly above that on the heated wall, i.e. here $T_{\max} > 1$. This situation continues to the higher values of Ra (Figs. 9d, 9e for $Ra = 300$, 500) with boundary layers developing on both the heated and cooled walls and with an almost stagnant central region. There is still a small region where the fluid temperature is above $T = 1$ for $Ra = 300$ (Fig. 9d) though here $T_{\max}$ is smaller than for $Ra = 40$ and $Ra = 100$. However, for $Ra = 500$ this region disappears with now $T_{\max} = 1$. Also at $Ra = 500$ the temperature within the main part of the flow region is almost independent of y. Again the results for higher values of p were found to be similar to those for $p = 1$.

4.3.3. Strong heating, $\gamma = 5.0$

To illustrate this case we take $\gamma = 5.0$. For $p = 1$ and $Ra = 0$ expression (22) gives $\gamma_0 = 2.4674$ and so $T_{\max} > 1$ with (22) giving $T_{\max} = 1.2711$ located at $y = 0.2975$ (away from the heated wall $y = 0$). This effect can be seen in Fig. 10a ($Ra = 0$), where the maximum flow rates now occur towards the cooled wall. For $Ra = 40$ (Fig. 10b) and $Ra = 100$ (Fig. 10c) the temperature and flow fields become distorted with stronger convective flows developing on the vertical walls (upwards on the heated wall and downwards on the cooled wall). The maximum temperature is still above $T = 1$ and is located on the top wall, though the value of $T_{\max}$ is reduced as Ra is increased, from $T_{\max} \simeq 1.201$ for $Ra = 40$ to $T_{\max} \simeq 1.053$

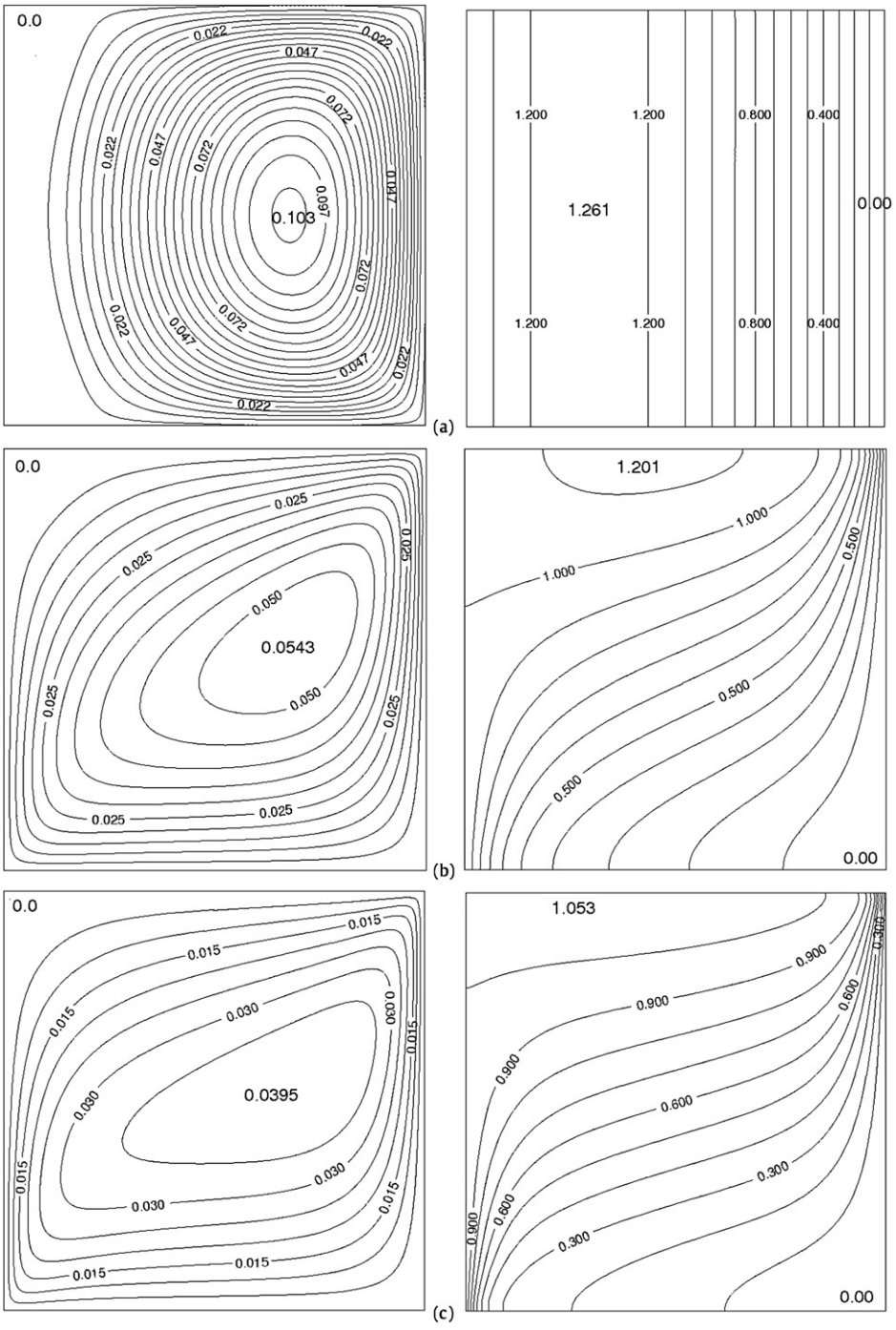

Fig. 10. Contour plots of the stream function and temperature for $\gamma = 5.0$, $p = 1$ and (a) $Ra = 0$, (b) $Ra = 40$, (c) $Ra = 100$, (d) $Ra = 300$, (e) $Ra = 500$.

for $Ra = 100$, though still noticeably greater than for the intermediate heating case. For $Ra = 300$ (Fig. 10d) and $Ra = 500$ (Fig. 10e) the same trends are seen as in the previous case, with boundary layers developing on the vertical walls and an almost stagnant flow in the central region. The value of $T_{\max}$ is further reduced, to $T_{\max} \simeq 1.005$ for $Ra = 500$, with the region where the temperature is above the heated wall value becoming smaller.

We considered this case for different values of p, with contour plots for $p = 2$ and $p = 5$ shown in Figs. 11 and 12, respectively. The same general trends are seen, the maximum temperature is above the heated wall value for all the Ra for which a (steady) solution is possible with this decreasing and moving towards the upper part of the heated wall as Ra is increased. The values of $T_{\max}$, for a given Ra, decrease slightly as p is increased, for example, for $Ra = 40$, $T_{\max} = 1.201$, 1.112 and 1.100 for $p = 1, 2$ and 5, respectively. The strength of the convective eddy flow also decreases slightly as p is increased. These results for the strong heating case ($\gamma = 5$) suggest that the value of p does not have a major effect on the flow and heat transfer within the porous medium in this case.

4.3.4. Total heat generation, Q

The main effect of the internal heating on the flow and heat transfer, on comparing with the results for $\gamma = 0$, are increased temperatures (which can be above the heated wall temperature) and stronger convective eddies. These differences are more pro-

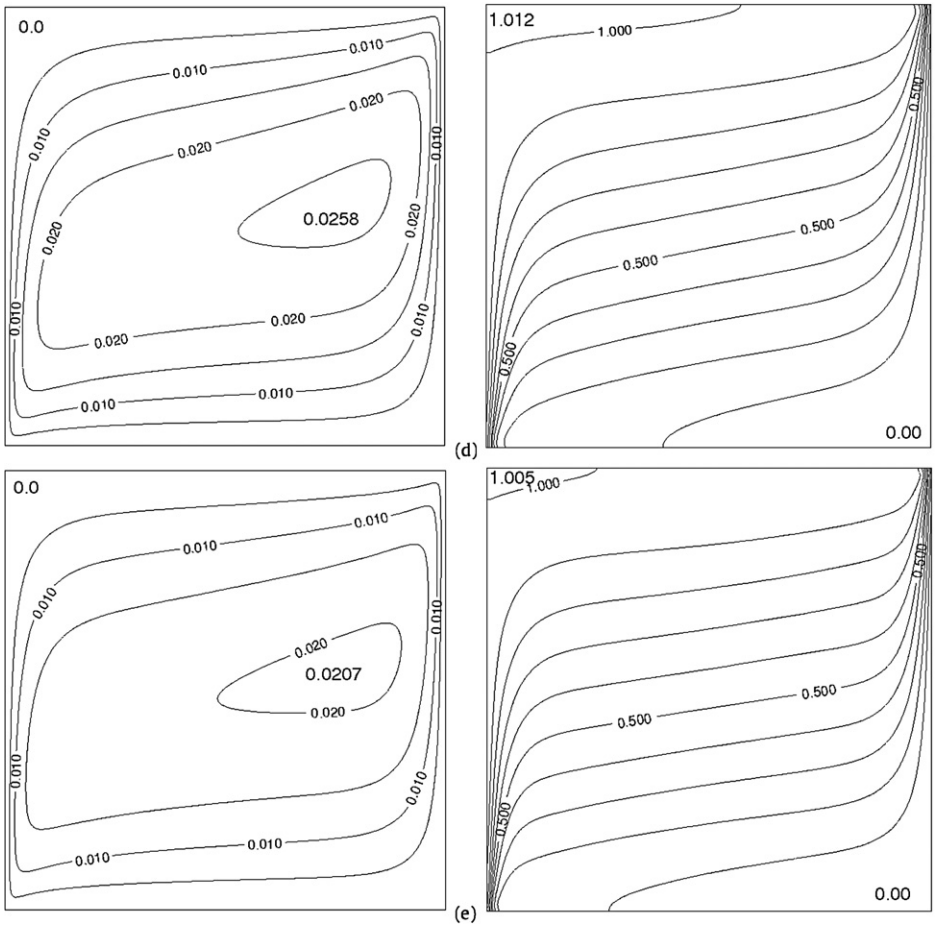

Fig. 10. (*continued*)

nounced as the value of γ is increased and become less significant as Ra is increased.

We can see this effect on the heat transfer in Fig. 13, where we plot Q, defined in (8), against Ra for different values of p and γ. For $p = 1$ and $p = 2$, Figs. 13a and 13b, respectively, Q decreases as Ra is increased for each of the values of γ tried. In both cases the total heat generated Q is above that for the case without any local heating, $\gamma = 0$, shown in Fig. 13a by a broken line. However, for $p = 5$, Fig. 13c, there is an increase in the total heat content Q for small Ra, with Q achieving a maximum value at a non-zero Ra before decreasing. This effect becomes more pronounced as γ is increased. These figures show that, for certain values of γ, p and Ra, significantly larger amounts of heat can be generated within the porous medium by the local heating, well above what would normally arise if this effect were not present.

5. Conclusion

We have considered the effects that internal heating at a rate proportional to the local temperature difference can have on the convective flow and heat transfer within a porous material. We have seen that there are three dimensionless parameters that describe this situation, namely a Rayleigh number Ra, a heating rate parameter γ and the exponent p in the local heating term. We started by considering the case $Ra = 0$, where the temperature field is independent of the flow. For this case we identified a critical value γ_c of γ, such that there were solutions possible only for $\gamma \leqslant \gamma_c$, with γ_c depending on p, see Figs. 2 and 3. This case also led to a value γ_0, where was a change in the maximum temperatures $T_{\max}$ achieved, see expressions (22), (24). For $\gamma < \gamma_0$ the temperature within the porous material was everywhere less than that on the heated wall, i.e. $T_{\max} = 1$. However, with $\gamma > \gamma_0$, temperatures above this can be generated by the local heating, i.e. $T_{\max} > 1$.

Our numerical results for $Ra > 0$ also showed the existence of a critical value γ_c for γ, see Fig. 4. We also identified a value γ_0 from our numerical results, with $T_{\max} > 1$ for $\gamma > \gamma_0$, see Fig. 7, with now γ_c and γ_0 dependent on both Ra and p. There appears to be a difference between the cases $p = 1$ and $p > 1$. For $Ra = 0$ the solution became unbounded at γ_c when $p = 1$, whereas there was a saddle-node bifurcation with the solution remaining bounded at γ_c when $p > 1$. This was also seen in the numerical results for $Ra > 0$ through not being able to 'join' these solutions to those for $Ra = 0$ with $p = 1$, see Fig. 6, at least for the very small values of Ra tried.

Our numerical results show that significantly higher temperatures can be generated by the internal heating, particularly for the larger values of γ, see Figs. 10–12. In these cases regions where the temperature is above the heated wall value $T = 1$ arise towards the top of the region and near the heated vertical wall and with stronger convective flows being set up, at least for moderate values of Ra. For larger values of Ra, boundary-layer flows develop on the vertical walls with a much weaker eddy flow in the central region. Thus for larger values of Ra, the internal heating becomes confined mainly to the upward flowing boundary layer on the heated wall and its overall effect is reduced, as can be seen in Figs. 5 and 13.

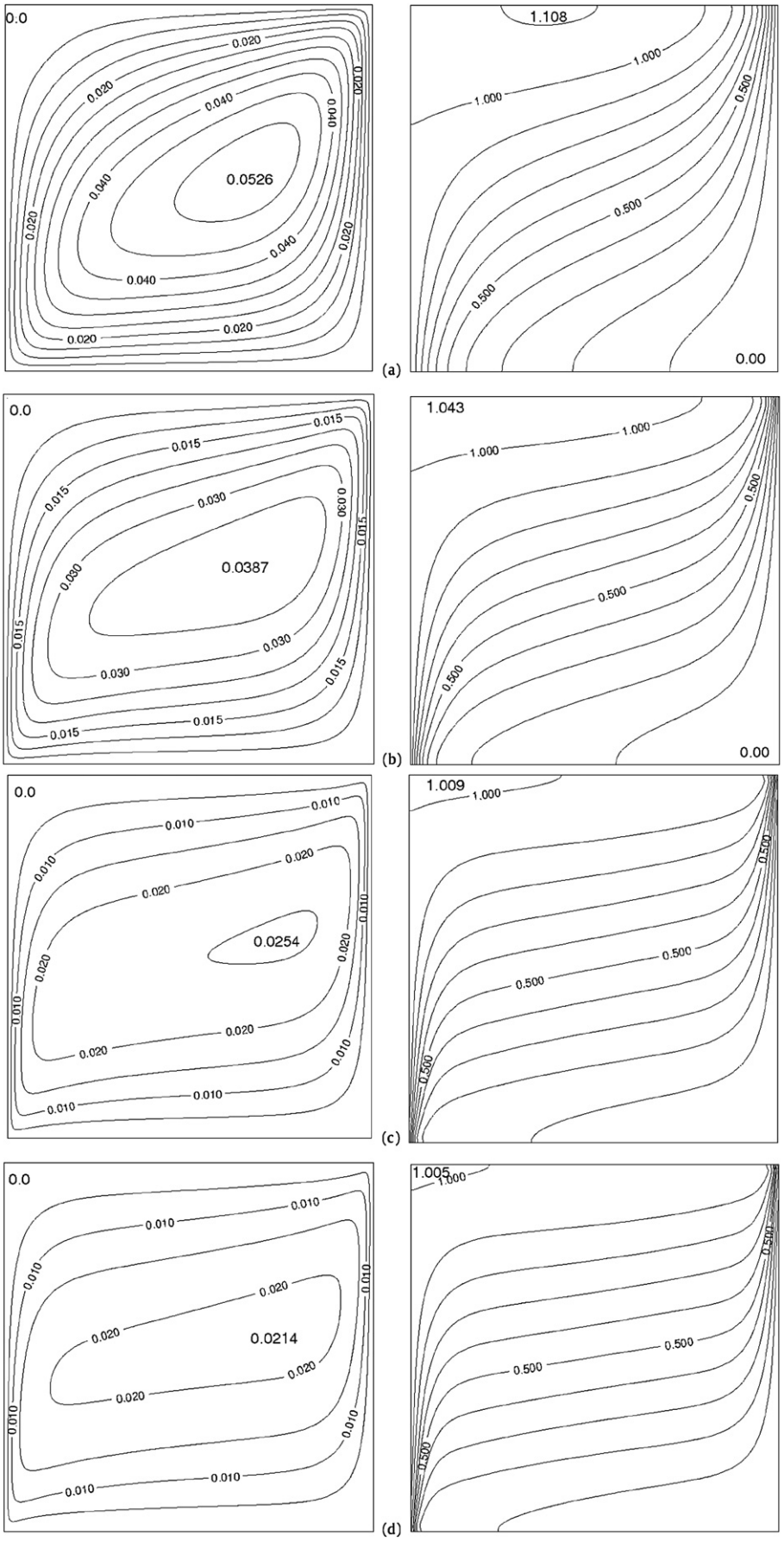

Fig. 11. Contour plots of the stream function and temperature for $\gamma = 5.0$, $p = 2$ and (a) $Ra = 40$, (b) $Ra = 100$, (c) $Ra = 300$, (d) $Ra = 500$.

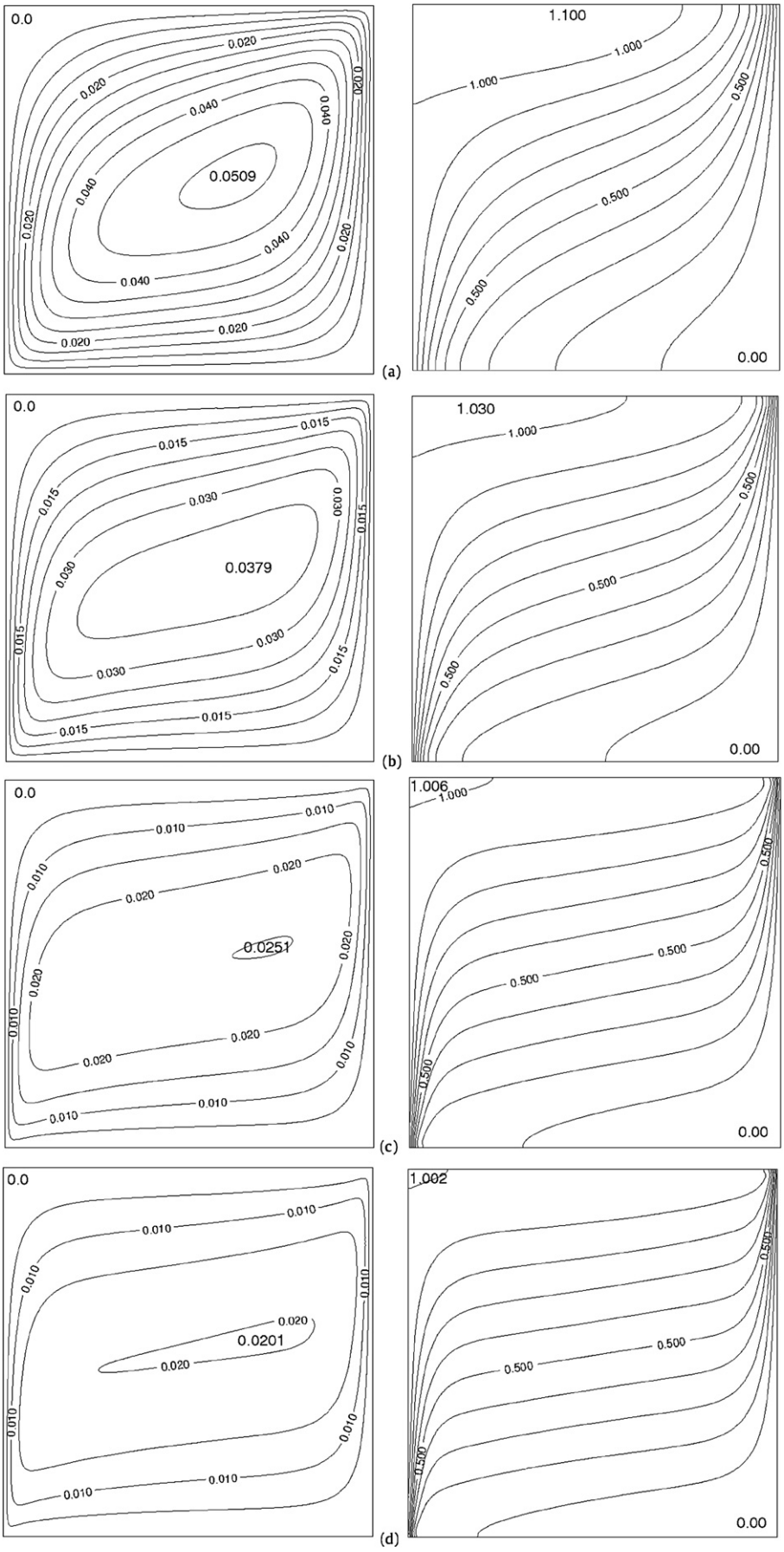

Fig. 12. Contour plots of the stream function and temperature for $\gamma = 5.0$, $p = 5$ and (a) $Ra = 40$, (b) $Ra = 100$, (c) $Ra = 300$, (d) $Ra = 500$.

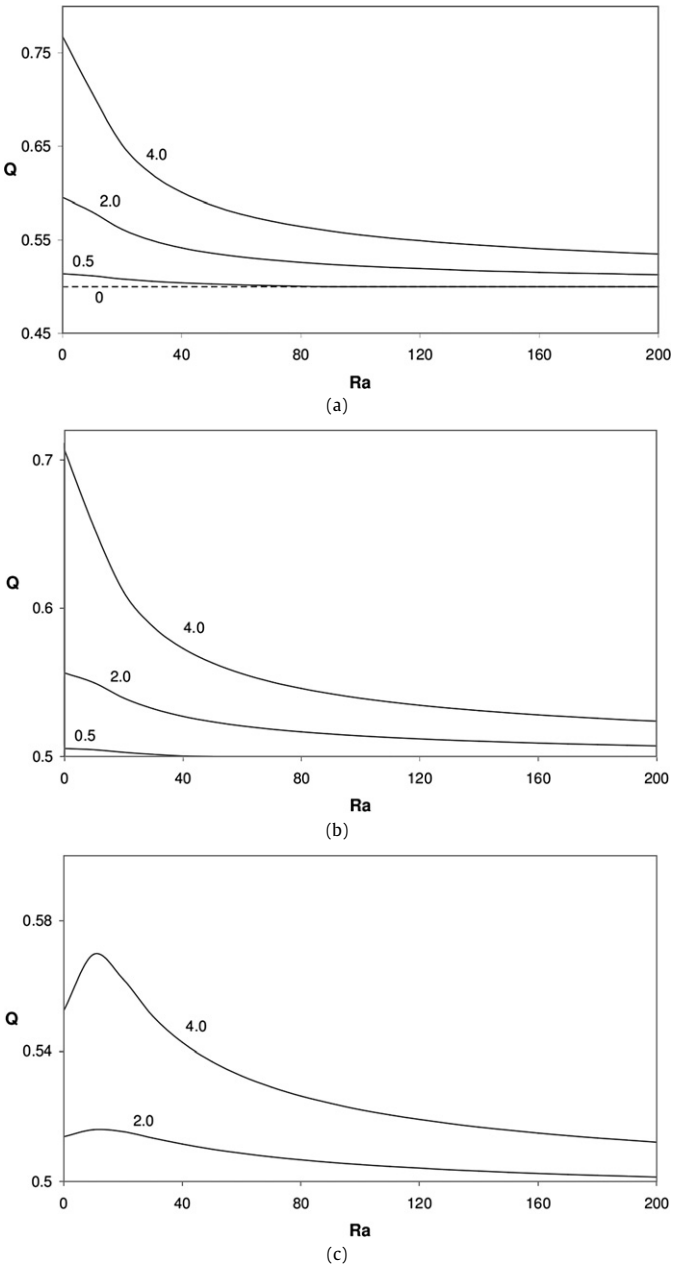

Fig. 13. Plots of the total heat content Q, defined in (8), against Ra for the values of γ labelled on the figure and for (a) $p = 1$, (b) $p = 2$, (c) $p = 5$. The broken line denotes the solution for $\gamma = 0$, no internal heating.

Acknowledgements

L.R.M. wishes to thank EPSRC for the Research Studentship which enabled this research to be undertaken. The authors also wish to thank Derek Ingham for encouraging us to consider this problem.

References

[1] D.A. Nield, A. Bejan, Convection in Porous Media, 3rd ed., Springer, New York, 2006.
[2] D.B. Ingham, I. Pop (Eds.), Transport Phenomena in Porous Media, Elsevier Science, Oxford, 1998.
[3] D.B. Ingham, I. Pop (Eds.), Transport Phenomena in Porous Media III, Elsevier Science, Oxford, 2005.
[4] K. Vafai (Ed.), Handbook of Porous Media, 2nd ed., Taylor and Francis, New York, 2005.
[5] I. Pop, D.B. Ingham, Convective Heat Transfer: Mathematical and Computational Modelling of Viscous Fluids and Porous Media, Pergamon, Oxford, 2001.
[6] D.B. Ingham, A. Bejan, E. Mamut, I. Pop (Eds.), Emerging Technologies and Techniques in Porous Media, Kluwer, Dordrecht, 2004.
[7] K. Brooks, D. Glasser, A simplified model of spontaneous combustion in coal stockpiles, Fuel 65 (1986) 1035–1041.
[8] K. Brooks, V. Balakotaiah, D. Luss, Effect of natural convection on spontaneous combustion of coal stockpiles, AIChE J. 34 (1988) 353–365.
[9] R.A. Sisson, A. Swift, G.C. Wake, B.F. Gray, The self-heating of damp cellulosic materials: I. High thermal conductivity and diffusivity, IMA J. Appl. Math. 49 (1992) 273–291.
[10] M.J. Sexton, C. Macaskill, B.F. Gray, Self-heating and drying in two-dimensional bagasse piles, Combustion Theory and Modelling 5 (2001) 517–536.
[11] B.F. Gray, M.J. Sexton, B. Halliburton, C. Macaskill, Wetting-induced ignition in cellulosic materials, Fire Safety Journal 37 (2002) 465–479.
[12] Transport Information Service: Cargo Loss Prevention, Information from German Marine Insurers: Pistachio Nuts. Die Deutschen Versicherer.
[13] S. Mahmud, R.A. Fraser, Free convection and irreversibility analysis inside a circular porous enclosure, Entropy 5 (2003) 358–365.
[14] M. Marcoux, M.-C. Charrier-Mojtabi, M. Azaiez, Double diffusive convection in an annular vertical porous layer, Int. J. Heat Mass Transfer 42 (1999) 2313–2325.
[15] B.V. Rathish Kumar, Shalini, Natural convection in a thermally stratified wavy vertical porous enclosure, Numerical Heat Transfer, Part A: Applications 43 (2003) 753–776.
[16] A.K. Singh, T. Paul, G.R. Thorpe, Natural convection in a non-rectangular porous enclosure, Forshung im Ingenieurwesen 65 (2000) 301–308.
[17] Y.F. Rao, B.X. Wang, Natural convection in vertical porous enclosures with internal heat generation, Int. J. Heat Mass Transfer 34 (1991) 247–252.
[18] M. Haajizadeh, A.F. Ozguc, C.L. Tien, Natural convection in a vertical porous enclosure with internal heat generation, Int. J. Heat Mass Transfer 27 (1984) 1893–1902.
[19] W.E. Stewart, M.E. Greer, L.A. Stickler, Heat transfer in a partially insulated rectangular enclosure of heat generating porous media, Int. Comm. Heat Mass Transfer 17 (1990) 597–607.
[20] M.V. Joshi, U.N. Gaitonde, S.K. Mitra, Analytical study of natural convection in a cavity with volumetric heat generation, ASME J. Heat Transfer 128 (2006) 176–182.
[21] E. Magyari, I. Pop, A. Postelnicu, Effect of the source term on steady free convection boundary layer flows over a vertical plate in a porous medium. Part I, Transport in Porous Media 67 (2007) 49–67.
[22] E. Magyari, I. Pop, A. Postelnicu, Effect of the source term on steady free convection boundary layer flows over a vertical plate in a porous medium. Part II, Transport in Porous Media 67 (2007) 189–201.
[23] NAG: Numerical Algorithm Group, web address: www.nag.co.uk.
[24] H. Jeffreys, B.S. Jeffreys, Methods of Mathematical Physics, Cambridge University Press, Cambridge, 1962.